Rotary Wing UAV: HIL tests for a model-based feedforward controller

Filippo Zanetti [1], Stefano Colautti [2], Gian Marco Saggiani[3], Veronica Rossi [4]

[1] Ph.D. candidate, University of Bologna, II School of Engineering - Forlì Campus
via Fontanelle 40, 47100 Forlì, Italy, e-mail: filippo.zanetti@unibo.it
[2] Ph.D. candidate, University of Bologna, II School of Engineering - Forlì Campus
via Fontanelle 40, 47100 Forlì, Italy, e-mail: stefano.colautti@unibo.it
[3] Associate Professor, University of Bologna, II School of Engineering - Forlì Campus
via Fontanelle 40, 47100 Forlì, Italy, e-mail: gianmarco.saggiani@unibo.it
[4] Graduate Technician, University of Bologna, II School of Engineering - Forlì Campus
via Fontanelle 40, 47100 Forlì, Italy, e-mail: veronica.rossi5@unibo.it

Key words: Rotary wing UAV, identification, model-based, feedforward, control.

Abstract. This paper presents the results of applying a model-based feedforward control technique to control a small scale unmanned Helicopter (RUAV). The very simple proposed architecture is based on nested proportional-integral control loops with the addition of a feedforward compensation in the inner loop. The feedforward term is obtained by the inversion of the command-attitude identified plant model. For a matter of comparison, a fast discrete time implementation will be also illustrated. An Hardware In the Loop (HIL) test bench will be presented and the velocity signal noise identification process will be illustrated. Finally stability analysis results and HIL simulations will show how this technique combines benefits of feedforward and feedback controllers and makes easier the tuning of the controller parameters.

Nomenclature

a, b	longitudinal and lateral rotor flapping
e	command-attitude transfer function gain coefficient
$e(t)$	white noise
g	(9.81 m/s^2) acceleration of gravity
p, q	roll, pitch rates
$y(t)$	noise in velocity signals
u, v, w	longitudinal, lateral and vertical speed
A_{lon} , B_{lat} , X_u , Y_v , X_a	on-axis derivatives
Y_b , L_b , M_a , Z_{coll},	on-axis derivatives
M_u , M_v , L_u , L_v	speed derivatives
A_{lat} , B_{lon} , M_b , L_a , M_{coll}	off-axis derivatives
$F(q)$	auto regressive polynomial filtering function
K_p , K_i , K_d	baseline inner loop PID parameters – Longitudinal
K_{pv} , K_{iv} , K_{dv}	baseline outer loop PID parameters – Longitudinal
K_{pLat} , K_{iLat} , K_{dLat}	baseline inner loop PID parameters – Lateral
K_{pvLat} , K_{ivLat} , K_{dvLat}	baseline outer loop PID parameters – Lateral
K_{pm} , K_{im}	feedforward inner loop PI parameters – Longitudinal
K_{pvm} , K_{ivm}	feedforward outer loop PI parameters – Longitudinal
K_{pmLat} , K_{imLat}	feedforward inner ioop PI parameters – Lateral
K_{pvmLat} , K_{ivmLat}	feedforward outer loop PI parameters – Lateral
T_{filt}, $T_{filtPhi}$	feedforward filter constants – Longitudinal, Lateral

θ, ϕ	longitudinal and lateral attitude angles
δ	command-attitude transfer function damping coefficient
δ_{lon} , δ_{lat}, δ_{coll}	cyclic longitudinal, lateral, collective control inputs
τ_e	main rotor time constant
ω_{np} , ω_{nq}	lateral, longitudinal fuselage-rotor-bar natural frequencies

Acronyms

AHRS – Attitude and Heading Reference System
FF – Feedforward
FFA – Feedforward Attitude
FMS – Flight Management System
HIL – Hardware In the Loop
RUAW – Rotary wing UAV
SISO – Single Input / Single Output
SS – States space

Appendix – Transfer functions

$BLG = CV(s)\cdot G_1(s)\cdot G_2(s)$ – Baseline Loop Gain (BLG)Transfer Function (TF)

$CA(s) = \dfrac{K_d\cdot s^2 + K_p\cdot s + K_i}{s}$ – PID Attitude Controller in Baseline control system

$CAM(s) = \dfrac{K_{pm}\cdot s + K_{im}}{s}$ – PI Attitude controller in Feedforward control system

$CV(s) = \dfrac{K_{dv}\cdot s^2 + K_{pv}\cdot s + K_{iv}}{s}$ – PID Velocity Controller in Baseline control system

$CVM(s) = \dfrac{K_{pvm}\cdot s + K_{ivm}}{s}$ – PI Velocity controller in Feedforward control system

$f = \dfrac{1}{1+T_{filt}\cdot s}$ – first order filter in Feedforward control system

$FFA = \dfrac{\delta_{lon}}{\theta} = \dfrac{-\tau_e}{A_{lon}}\cdot\dfrac{s^3+1/\tau_e\cdot s^2+{\omega_{nq}}^2\cdot s}{{\omega_{nq}}^2}$ – Feedforward action, Longitudinal

$FFA = \dfrac{\delta_{lat}}{\phi} = \dfrac{\tau_e}{B_{lat}}\cdot\dfrac{s^3+1/\tau_e\cdot s^2+{\omega_{np}}^2\cdot s}{{\omega_{np}}^2}$ – Feedforward action, Lateral

$FLG(s) = G_{ff}(s)\cdot CVM(s)$ – FF Loop Gain

$FTF(s) = \dfrac{FLG(s)}{1+FLG(s)}$ – FF Transfer Function

$G_1(s) = \dfrac{CA(s)\cdot P(s)}{CA(s)\cdot P(s)+1}$

$G_2(s) = \dfrac{\pi}{180}\cdot\dfrac{u(s)}{\theta(s)}$, $G_2(s) = \dfrac{\pi}{180}\cdot\dfrac{v(s)}{\phi(s)}$ – Longitudinal, Lateral attitude-velocity TF, derived from SS model

$Gff(s) = G_{fff1}(s)\cdot G_2(s)$

$G_{fff1}(s) = f\cdot\dfrac{CAM(s)\cdot P(s)+FFA(s)\cdot P(s)}{CAM(s)\cdot P(s)+1}$

$P(s) = \dfrac{\theta(s)}{\delta_{lon}(s)}$, $P(s) = \dfrac{\phi(s)}{\delta_{lat}(s)}$ – Longitudinal, Lateral command-attitude TF, from SS model

A. Introduction and system description

The successful application of UAV (Unmanned Arial Vehicle) systems, both for civil and for military application, depends greatly on their level of controllability and flying qualities. The control of small scale helicopter (Rotorcraft UAV, RUAV), in order to maintain a stable attitude and to follow a desired trajectory, is particularly critical since it is well known that helicopters are inherently unstable systems. A good number of papers have been written in the last years about methodologies for increasing the limited performances of this class of small scale helicopters, but only few of them have used the identified dynamic models to support advanced control design [1].

In the last years UNIBO has developed an unmanned small scale helicopter [2] that is now capable of autonomous flight and that can be used as a platform for researches in control and navigation laws.

This paper presents the results achieved at the Aerospace Laboratories of the University of Bologna (Italy), concerning the validation of an innovative model-based feedforward (FF) controller for Rotary Wing UAV in a Hardware In the Loop (HIL) test bench.

The UNIBO RUAV, shown in figure 1, is built around a modified Hirobo Eagle II 60 hobby helicopter with a more powerful engine, longer fiberglass blades, both for the main and the tail rotor, and longer tail boom. The new main rotor is a 2 blades see-saw type rotor with Bell-Hiller stabilizer bar and a 1.84 m diameter; the helicopter total mass is about 11.2 kg. A National Instruments CompactRIO system has been selected as flight computer and performs both the task of Autopilot and Flight Management System (FMS). For flight data acquisition a Crossbow NAV420 GPS-aided Attitude and Heading Reference System (AHRS) and ultrasonic sensors have been installed to provide accurate signals in velocity, altitude and helicopter attitude.

The on-board computer NI compactRio is programmed using Labwiev coding language that allows quick set up of different control logic algorithms. In a first step a traditional PID controller [2,3] has been implemented, while recently the proposed advanced controller based on feedforward action has been coded.

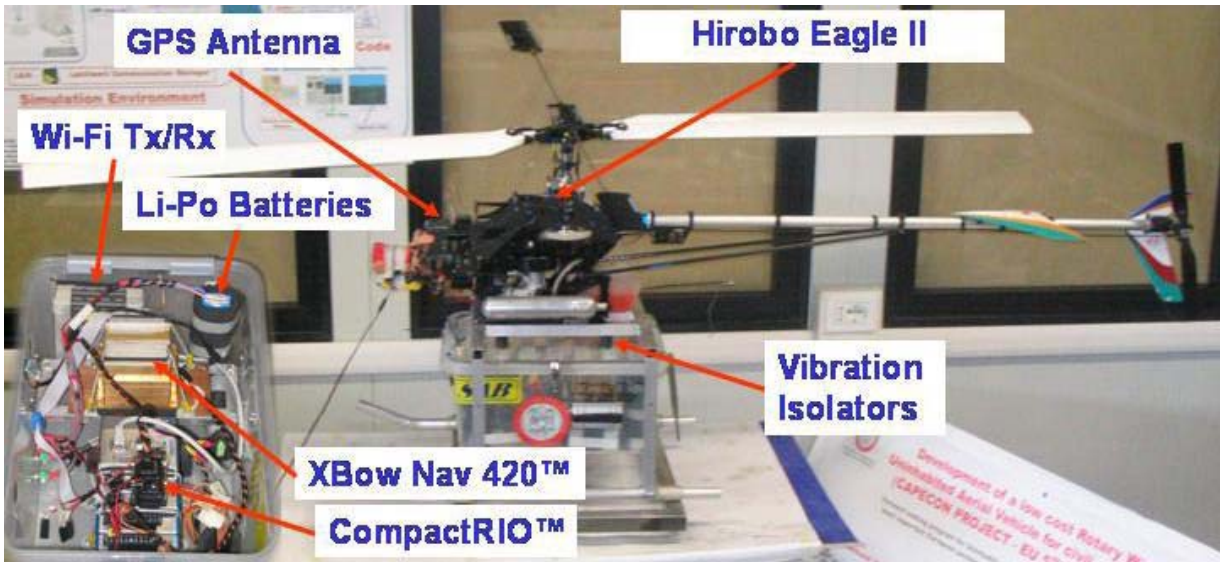

Fig. 1: UNIBO Rotary wing UAV

In the following control performances of this innovative model-based Feedforward controller will be compared with those of a Baseline control system.

B. Baseline and FF controllers architectures

In both cases separate Single-Input/Single-Output (SISO) control systems are used for lateral and longitudinal dynamics control: the outer control loop uses helicopter target and measured velocities to produce the reference for the inner attitude loop and the inner attitude loop computes commands (δ_{lon}, δ_{lat}) using outer loop attitude references (θ_{ref} , ϕ_{ref}) and measured helicopter attitude feedbacks (θ , ϕ) . The vertical position and the heading are controlled by two separate PID single loop controllers.

Baseline controller for longitudinal and lateral dynamics consists in a SISO PID control with a two levels nested loop structure (see fig. 2). Lateral and longitudinal track velocities errors are used in the *CV* blocksets to generate respectively demands for the roll (ϕ) and the pitch (θ) attitude control module (*CA* blocksets),

A block diagram of a SISO controller for the Baseline control system is represented in Fig. 2.

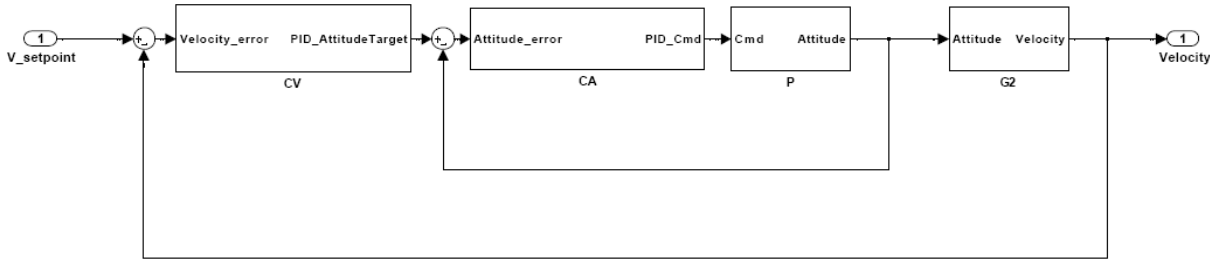

Fig 2: Block diagram of the Baseline controller for longitudinal or lateral dynamics

The proposed FF control architecture (see fig. 3) is very simple and it is based on SISO nested control loops in which the outer loop consists of a PI controller (*CVM* blockset), while the inner loop is a FeedForward + Proportional and Integral controller (*FFA+CAM* blockset): the attitude feedforward term (*FFA*) is obtained by the inversion of the attitude identified linear model, as described in the next paragraph.

The output of the PI velocity controller (*CMV* blockset) is filtered by means of a first order filter (*f* blockset) with dedicated time constants for longitudinal and lateral controllers (T_{filt}, $T_{filtPhi}$).

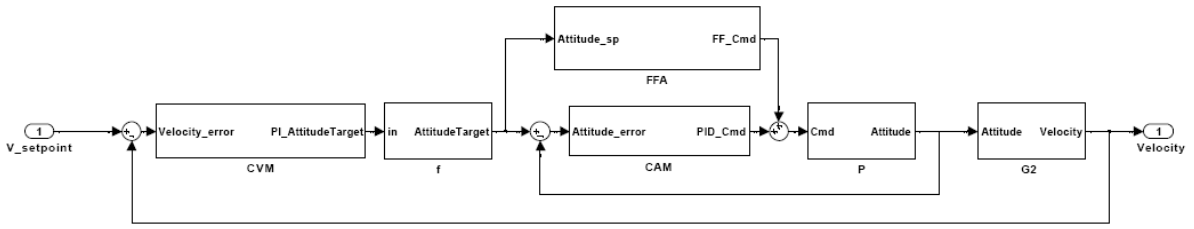

Fig 3: Block diagram of the FF controller for longitudinal or lateral dynamics

The discrete sampling time has been fixed in 0.020 seconds both for lateral and longitudinal dynamics.

C. Discrete-time implementation of *FF+PI* control model

In *FF+PI* controller, the feed forward attitude (FFA) term, as already mentioned, can been obtained by inverting the plant identified command-to-attitude transfer function. Neglecting cross-effects, this transfer function is a third order system formed by the product of a pure integrator term and a second order transfer function [4]:

$$\frac{\theta}{\delta_{lon}} = \frac{-A_{lon}}{\tau_e} \cdot \frac{1}{s} \cdot \frac{\omega_{nq}^{\ 2}}{s^2 + s/\tau_e + \omega_{nq}^{\ 2}}; \quad \frac{\phi}{\delta_{lat}} = \frac{B_{lat}}{\tau_e} \cdot \frac{1}{s} \cdot \frac{\omega_{np}^{\ 2}}{s^2 + s/\tau_e + \omega_{np}^{\ 2}} \quad (1)$$

A unique formulation, valid for longitudinal and lateral dynamics, can be expressed by:

$$P(s) = \frac{1}{s} \cdot \frac{e \cdot \omega_n^{\ 2}}{s^2 + 2 \cdot \delta \cdot s + \omega_n^{\ 2}} \qquad (2)$$

where delta δ is the damping coefficient, ω_n is the natural frequency and e is the gain of the second order transfer function.
Comparing relations (1) and (2), for longitudinal dynamic following relations can be written:

$$e = -\frac{A_{lon}}{\tau_e} \qquad \delta = \frac{1}{2 \cdot \tau_e \cdot \omega_{nq}} \qquad \omega_n = \omega_{nq}$$

whereas for lateral dynamic:

$$e = \frac{B_{lat}}{\tau_e} \qquad \delta = \frac{1}{2 \cdot \tau_e \cdot \omega_{np}} \qquad \omega_n = \omega_{np}$$

Hence in the continuous time domain, the feed forward contribute (*FFA*) will be written as the inverse of *P(s)*:

$$FFA = P(s)^{-1} = \frac{s^3 + 2 \cdot \delta \cdot s^2 + \omega_n^{\ 2} \cdot s}{e \cdot \omega_n^{\ 2}}$$

while turning into the discrete time domain, using Backward approximation [5], the command δ_k to be actuated can be computed (k index is related to the sample time instant):

$$\delta_k = \frac{1}{e \cdot \omega_n^{\ 2}} \left[\frac{1}{T_s^{\ 3}} \left(u_k - 3 \cdot u_{k-1} + 3 \cdot u_{k-2} - u_{k-3} \right) + \frac{2 \cdot \delta}{T_s^{\ 2}} \left(u_{k-1} - 2 \cdot u_{k-2} + u_{k-3} \right) + \frac{\omega_n^{\ 2}}{T_s} \left(u_{k-2} - u_{k-3} \right) \right] \qquad (3)$$

In the longitudinal control, for example, if $u_k = \theta_{ref\_k}$, or, in other words, if the input u_k is the filtered attitude set-point generated by the *CVM* blockset, then eq. 3 computes the command $\delta_{long\_k} = \delta_k$ that would bring the modeled system to perfectly track its original set-point θ_{ref_k}, in total absence of disturbances.

Note that, the sampling time T_s for feedfoward term has been selected in 0.040 s, whereas all the other variables continue to be updated every 0.020 s. This choice has been driven by the necessity of bounding the derivatives in eq. 1 as a consequence of the relatively low resolution of the velocity signal computed by the inertial unit Crossbow NAV420.

D. Hardware in the loop test bench and Unibo RUAV dynamic model

D.1 Helicopter dynamic model

The helicopter dynamics State Space Model adopted in the HIL has been identified in the time domain with a particular procedure [3] and can be represented as follows:

$$\dot{x} = A \cdot x + B \cdot u$$
$$y = C \cdot x + D \cdot u$$

where input command vector is: $u = [\delta_{lon}, \delta_{lat}, \delta_{coll}]^T$

the state vector is: $x = [u, v, p, q, \phi, \theta, a, b, w]^T$

the output vector is: $y = [u, v, p, q, \phi, \theta, w]^T$

and:

$$A = \begin{bmatrix} X_u & 0 & 0 & 0 & 0 & -g & X_a & 0 & 0 \\ 0 & Y_v & 0 & 0 & g & 0 & 0 & Y_b & 0 \\ L_u & L_v & 0 & 0 & 0 & 0 & L_a & L_b & 0 \\ M_u & M_v & 0 & 0 & 0 & 0 & M_a & M_b & 0 \\ 0 & 0 & 1 & 0 & 0 & 0 & 0 & 0 & 0 \\ 0 & 0 & 0 & 1 & 0 & 0 & 0 & 0 & 0 \\ 0 & 0 & 0 & -1 & 0 & 0 & -1/\tau_f & A_b/\tau_f & 0 \\ 0 & 0 & -1 & 0 & 0 & 0 & B_a/\tau_f & -1/\tau_f & 0 \\ 0 & 0 & 0 & 0 & 0 & 0 & 0 & 0 & Z_w \end{bmatrix} \quad B = \begin{bmatrix} 0 & 0 & 0 \\ 0 & 0 & 0 \\ 0 & 0 & 0 \\ 0 & 0 & M_{coll} \\ 0 & 0 & 0 \\ 0 & 0 & 0 \\ A_{lon}/\tau_f & A_{lat}/\tau_f & 0 \\ B_{lon}/\tau_f & B_{lat}/\tau_f & 0 \\ 0 & 0 & Z_{coll} \end{bmatrix}$$

Aerodynamic derivatives numerical values are indicated in table 1.

A_{lon}	0.2488 rad/rad		X_u	0.052 1/s		X_a	9.81 m/(s^2·rad) (constrained)		Z_w	– 0.3567 1/s
B_{lat}	0.22 rad/rad		M_u	– 0.0026		L_a	123.36		Z_{coll}	– 7.733 m/(s^2·rad)
A_{lat}	0.105		L_u	3.8 e–4		M_a	146.4 1/s^2		M_{coll}	– 17.09
B_{lon}	3.2 e–4		Y_v	0.046 1/s		Y_b	9.81 m/(s^2·rad) (constrained)		t_f	0.132 s
A_b	Set to 0		L_v	– 0.0013		L_b	327.6 1/s^2		g	9.81 m/s^2
B_a	Set to 0		M_v	– 9.0 e–4		M_b	– 81.851			

Table 1: Identified derivatives values for Unibo RUAV

D.2 Disturbances and sensor noise model

The dynamic model described in the previous section predicts only the low frequency response of the helicopter (approximately under 5Hz), while real signals acquired by onboard sensors present also higher frequency noise values. Analyzing the power spectral density (PSD) of speed signals acquired during several flight tests (fig. 4), it can be noticed the presence of well distinct peaks at 34 Hz, corresponding to the double of main rotor revolution frequency ($\omega_n \cong 17Hz$ corresponding to about 1000 rpm).

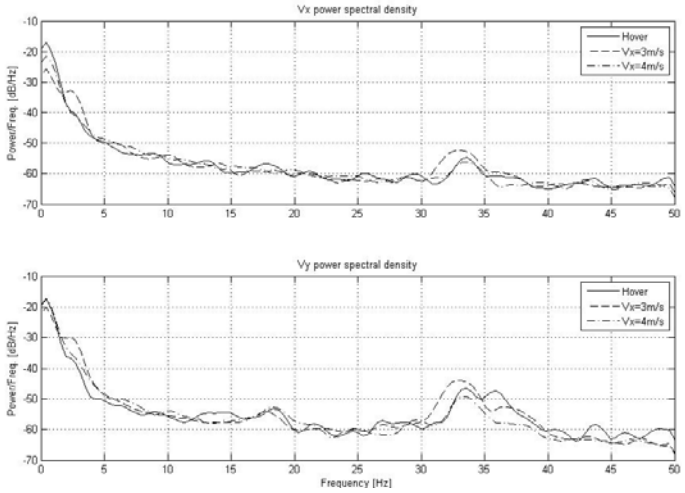

Fig. 4 Power spectral density of longitudinal and lateral velocity signals

This high frequency noise in attitude and speed signals can downgrade the controller performances. In order to have a more realistic prediction of the controller behavior during HIL tests, a model of these disturbances should be added to the state space model helicopter dynamics. The effect of noise attitude and speed signals has been predicted by calculating the closed loop transfer functions between a injected disturbance on attitude (*na(s)*) or speed (*nu(s)*) and the consequent speed disturbance (*u(s)*).

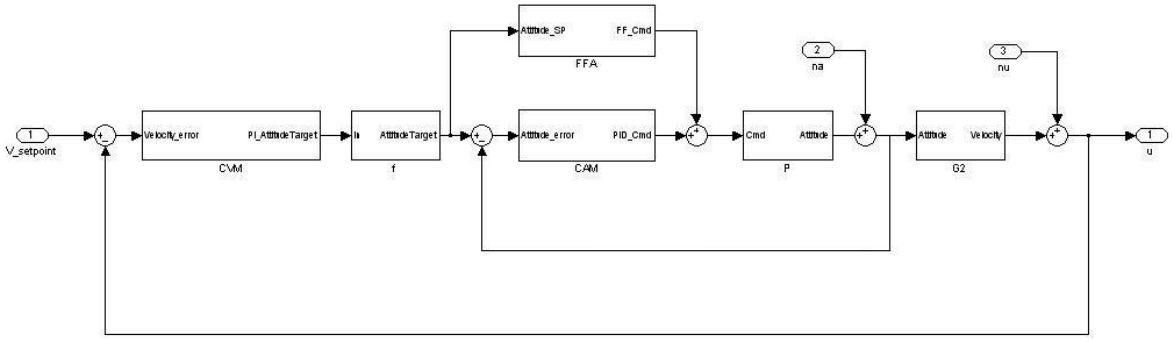

Fig. 5 Block diagram of the FF controller with noise injection

Referring to figure 5, the transfer function between "noise on attitude" and speed is:

$$\frac{u(s)}{na(s)} = \frac{G_2(s)}{1 + P(s)\cdot(CAM(s)\cdot(1 + G_2(s)\cdot CVM(s)\cdot f(s)) + FFA(s)\cdot G_2(s)\cdot CVM(s)\cdot f(s))} \tag{4}$$

and the transfer function between "noise on speed" and speed output is:

$$\frac{u(s)}{nu(s)} = \frac{1 + CAM(s) \cdot P(s)}{1 + P(s) \cdot CAM(s) + G2(s) \cdot P(s) \cdot CVM(s) \cdot f(s) \cdot (FFA(s) + CAM(s) \cdot)} \quad (5)$$

Same relations are valid both for Feedforward and for the Baseline controller setting, but, for the latter, it has to be set:

$$f(s) = 1,\ FFA(s) = 0$$

Bode plots of eq.4 and 5 have been reported in Fig.6 and Fig.7.

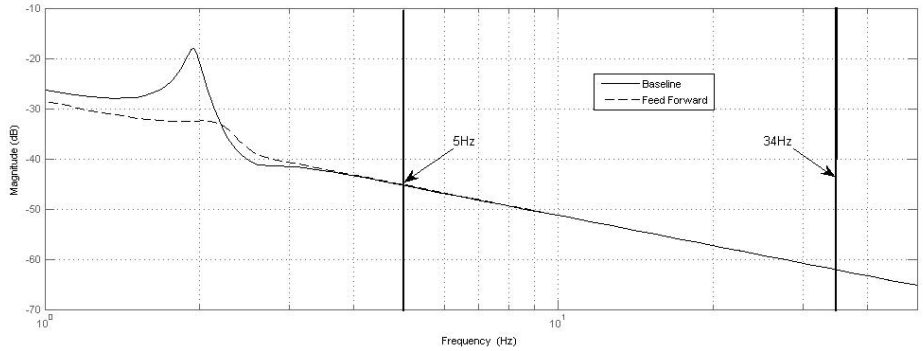

Fig. 6 Bode plot of velocity -'noise on attitude' transfer function (*u(s)/na(s)*)

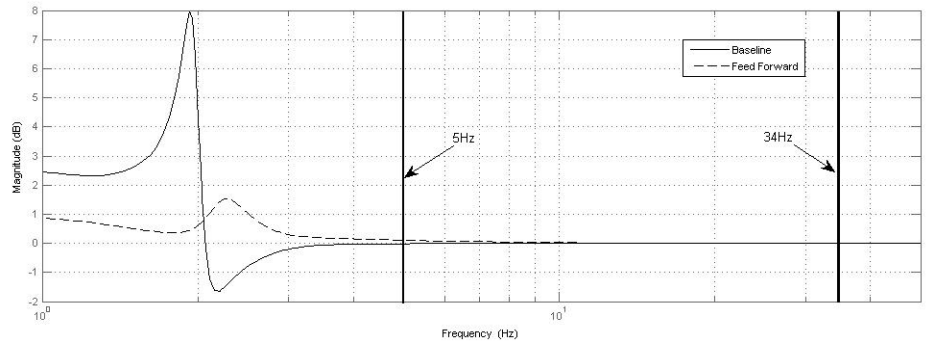

Fig. 7 Bode plot of velocity -'noise on velocity' transfer function (*u(s)/nu(s)*)

As it can be seen in fig. 6, all the disturbance frequencies in the attitude signal are heavily damped by the system and will have only small influence on controller performances.
In the case of noise injected in velocity, instead, figure 7 shows that the high frequencies remain unaltered and can still disturb the controller. This analysis leads to the conclusion that it is necessary to model the high frequencies of speed noise in order to have a more realistic prediction of the controller performances during the real flight tests, while noise on attitude in not necessary. Moreover modeling 'noise on velocity' appears to be critical especially for Feedforward controller which operates derivatives (eq.3) with velocity speed error signals without tunable gains.
The PSD of the speed signals shows that there is no correlation between the noise characteristics and the flight command inputs; for this reason Auto Regressive structure (AR) [6] has been chosen to model these disturbances.

In general, the AR model can be written as:

$$F(q)\cdot y(t) = e(t)$$
$$F(q) = 1 + f_1 q^{-1} + ... + f_n q^{-n} \qquad (6)$$

where $y(t)$ is the output signal at time t, $e(t)$ is a white noise and q is a delay operator. Identification of $f_1.....f_n$ parameters has been performed using a least square method starting from flight data previously filtered in order to eliminate the low frequency values, which are still modeled by state space model. The polynomial order, which is the only free parameter in this approach, has been fixed equal to 30, because, previous tests have revealed that this value represents a good compromise between accuracy and computational effort.

Fig 8 shows the result of the identification process. Data used for the identification process were the one with the higher power at 33Hz (flight test with longitudinal speed at 3m/s). As it can be seen, all the main characteristics of the noise PSD have been predicted with high accuracy, bringing to a good statistical model of the noise.

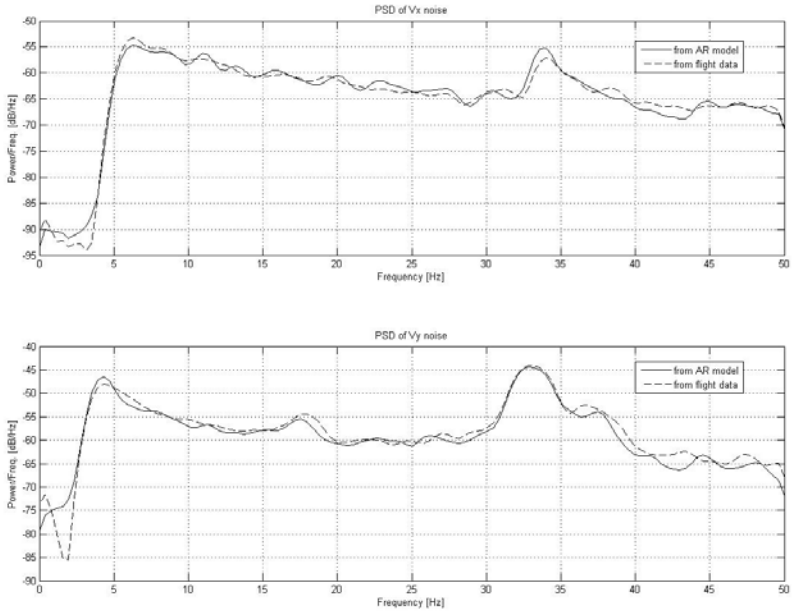

Fig. 8 Comparison between modeled (dashed) and original (continuous) flight data PSD

The HIL global model is composed of a state space model which predicts only the signal frequencies under 5Hz and of an AR model which simulate the remaining frequencies between 5Hz and 50Hz.

D.3 Hardware in the loop test bench

To asses the performance of the two different controllers, an Hardware In the Loop test bench was developed and its architecture is illustrated in figure 9 (right side).

It is composed by:
- A CRIO, equal to the onboard one, which runs the control software;
- an FPGA module which acquires PWM commands (PXI 7831);
- a computer which emulates the helicopter plant and the onboard sensor outputs.

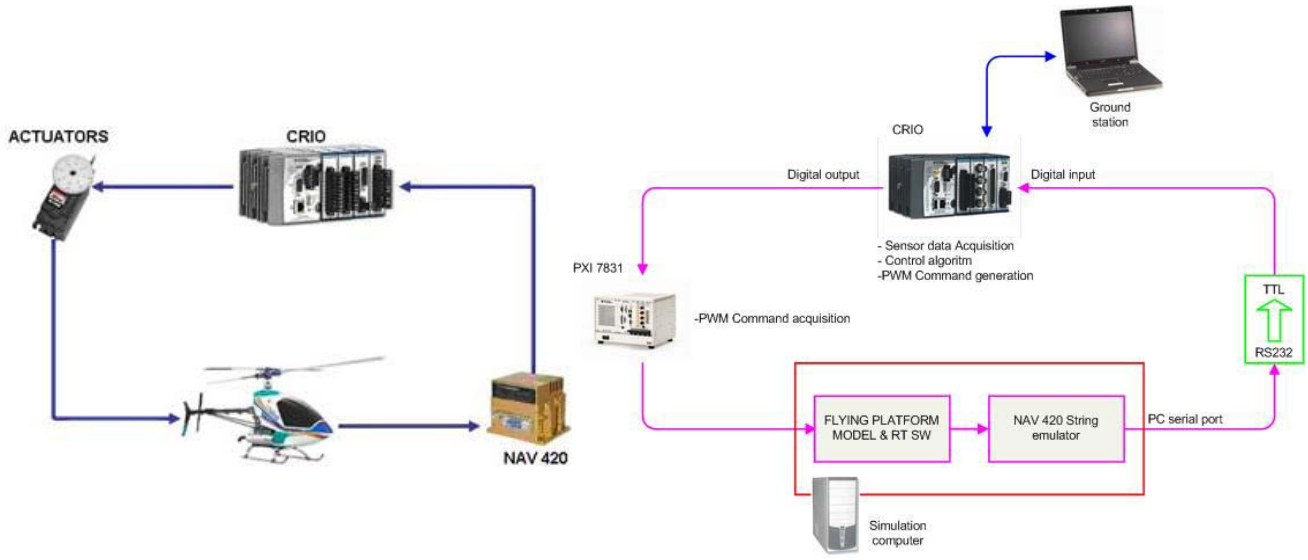

Fig 9:Real control loop (left) and Hardware in the loop test bench (right)

CompactRIO digital outputs, that usually drive the servo actuators, are acquired, in the HIL test bench, by the PXI FPGA module and converted in degrees of servo control actuation.
On the simulation computer a NI Labview software implements the state space and noise models illustrated before. That module computes, in real time, the helicopter response due to control input. A NAV420 emulator simulates the original serial data packet format and is used to send information to the main controller.
Since PC serial port uses RS232 signals and CRIO digital inputs accept TTL voltage levels, an integrated circuit board has been placed between computer output and CRIO input.
The helicopter ground station can be connected to the HIL for sending to the controller the desired speed profile, or any kind of commands, and to save helicopter outputs: these outputs are then used for assessing the controller performances.

E. Baseline and FF Controllers Automatic tuning

In order to make an impartial analysis of controllers goodness, in terms of stability and performances, an automatic tuning strategy, in house developed and based on step response characteristics, has been adopted. In this way, Baseline and Feedforward controllers have been automatically tuned in order to have same performances in the response to a unitary (1 m/s) velocity step.

Table 2 reports the constraints values used.

	Rise Time	% Rise	Settling Time	% Settling	% Overshoot	% Undershoot
Longitudinal/Lateral	1. 0 /1.2 (s)	90%	2.5	2%	2%	2%

Table 2: Response characteristics for longitudinal and lateral dynamics

The meaning of the constraints reported in table 2 is more clearly defined in figure 9.

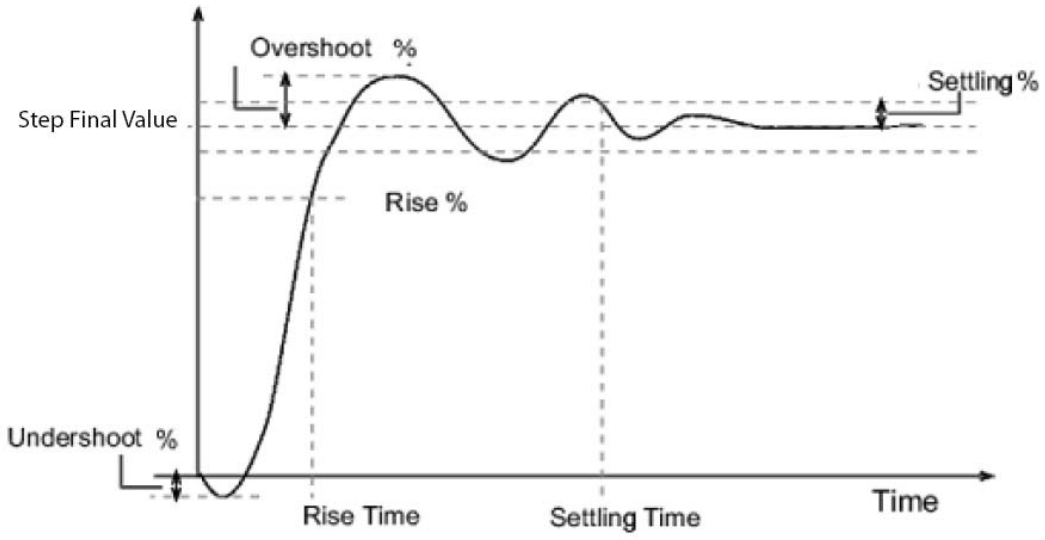

Fig. 9: Unitary step response characteristics

Referring to table 2, it has to be noticed that a very small overshoot requirement has been chosen to fulfill the ADS33 [7] hover and low speed specification (cit. *"There shall be no noticeable overshoots in the response of translational rate to control"*) and that settling percentage has been set to the same value of overshoot in order to obtain a first order response as prescribed by the norms.

With the adopted automatic tuning procedure and the above constraints it has been possible to find the controllers gains reported in table 3.

	Baseline Longitudinal	**Baseline Lateral**	**FF Longitudinal**	**FF Lateral**
Attitude Proportional	$K_p = -2.0062$	$K_{pLat} = 2.4$	$K_{pm} = -1.0336$	$K_{pmLat} = 1.9068$
Attitude integral	$K_i = -4.5837$	$K_{iLat} = 1.44$	$K_{im} = -2.1015$	$K_{imLat} = 1.2618$
Attitude derivative	$K_d = 0$	$K_{dLat} = 0.06$	--	--
Velocity Proportional	$K_{pv} = -11.3730$	$K_{pvLat} = 7.9685$	$K_{pvm} = -9.5234$	$K_{pvmLat} = 9.5498$
Velocity integral	$K_{iv} = -0.6914$	$K_{ivLat} = 0.410$	$K_{ivm} = -0.3864$	$K_{ivmLat} = 0.3442$
Velocity derivative	$K_{dv} = -1.1017$	$K_{dvLat} = 0.0077$	--	--
Filter time constant	--	--	$T_{filt} = 0.1117$	$T_{filtLat} = 0.2187$

Table 3: Response characteristics for longitudinal and lateral dynamics

F. Stability analysis

Stability analysis has been performed by computing Gain and Phase stability margins [4] for the Baseline and the Feedforward control systems. The two Loop Gain transfer functions for longitudinal and lateral controllers have been derived from control schemes depicted in fig. 2 and fig. 3 and automatically computed unknown parameters have been used. Bode diagrams of Loop Gain transfer functions BLG and FLG are reported in Fig.10, in which stability margins have been indicated by means of circular markers.

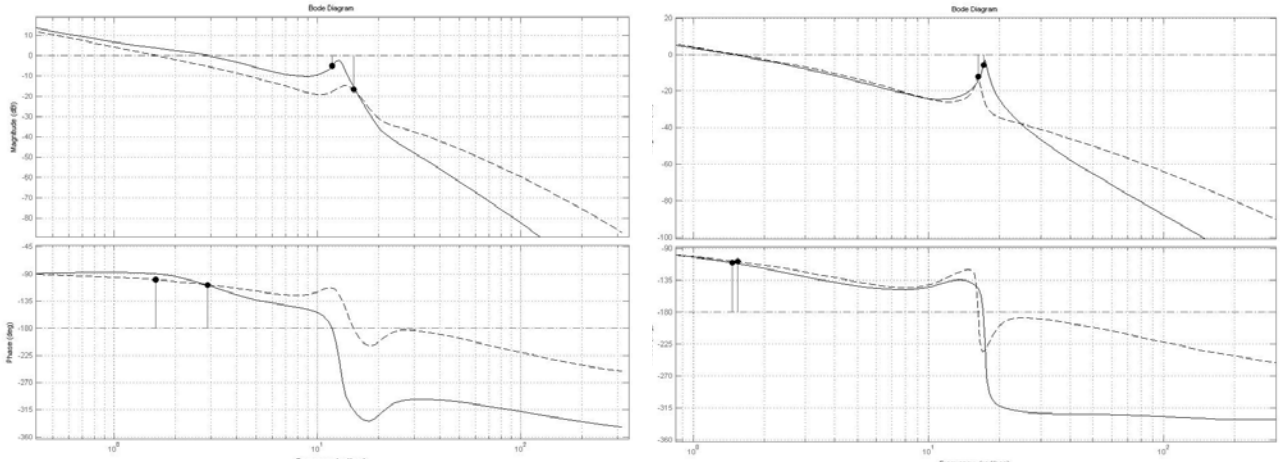

Fig. 10 Bode Diagrams for Stability analysis. Longitudinal (left), Lateral (right) dynamic; Baseline (continuous line) and Feedforward (dashed line) controller

Bode magnitude and phase diagrams are reported in figure 10 for Baseline Loop Gain (BLG) and the FF Loop Gain (FLG) transfer functions both for longitudinal (left) and lateral (right) dynamics appear to be very similar to those reported in literature [4].

Looking at these figures it can be seen that, in both cases, the feedforward architecture assures an improvement of phase and stability margins. In fact, for the Baseline controllers the critical frequencies for stability (11.8 rad/sec for the longitudinal, 17.1 rad/sec for the lateral dynamic) almost coincide with the natural frequency of the lightly damped coupled rotor/stabilizer/fuselage group caused by the stabilizer bar (12.1 rad/sec for the longitudinal and 18 rad/sec for the lateral dynamic [1]) and this brings to a great reduction in the gain margin.

The effect of the FF compensation brings to a reduction in the lightly damped coupled rotor/stabilizer/fuselage influence and, hence, to an improvement of gain margin.
Gain and Phase stability margins are finally reported in table 4.

		Gain margin (dB)	**Phase margin (deg)**
Baseline	**Longitudinal**	5.24 dB (@ 11.8 rad/sec)	71.6 deg (@ 2.88 rad/sec)
	Lateral	5.54 dB (@ 17.1 rad/sec)	69.8 deg (@ 1.47 rad/sec)
Feedforward	**Longitudinal**	16.9 dB (@ 15 rad/sec)	80.2 deg (@1.61 rad/sec)
	Lateral	12.1 dB (@ 16.2 rad/sec)	71.6 deg (@1.54 rad/sec)

Table 4: Stability margins of the FF and Baseline controllers for longitudinal and lateral dynamics

It has to be noticed that only FF controller fulfils the specifications for flight control design [7], which require a gain margin of 6 dB and a phase margin of 45 deg, whereas the Baseline control system lacks adequate Gain margin.

This stability analysis, moreover, doesn't take into account noise effects and problems due to quantisation of the analogue signals that slightly affect final performances and that will be analyzed in next section.

G. HIL tests

The Baseline and Feedforward control systems tuned with the parameters reported in the previous section, have been tested in the Hardware in The Loop test bench described in fig. 8. The dynamic model of paragraph C.1 has been used coupled with the velocity signal noise (par. C.2).

HIL tests results are reported in next figures and confirm the stability analysis described in paragraph F. In Fig 11 are depicted the axial velocity, pitch attitude (baseline and FF) and the longitudinal command, related to an unitary velocity step for the two controllers. Whereas the controllers have been automatically tuned in order to attain the same velocity performances, a small difference in performance can be anyway observed, like, for example, a smaller rise time for the Baseline velocity response. This is probably due to the automatic tuning procedure that has set up a slightly faster solution for Baseline controller. Another reason for this difference can be found in small differences between the Simulink dynamic and control models used during tuning sessions and in the HIL test bench that is entirely coded in Labview. Contrary result occurred in lateral controller tuning where Baseline controller resulted slightly lower than FF but, anyway, the differences between the velocity responses are small and they do not invalidate our comparison.

In the second and third strips of the same figure, it can see that the Baseline attitude and actuation command signals oscillate, whereas the feedforward ones are much more stable. This appears to be consistent with the consideration reported in previous paragraph, about the smaller gain margin of Baseline system.

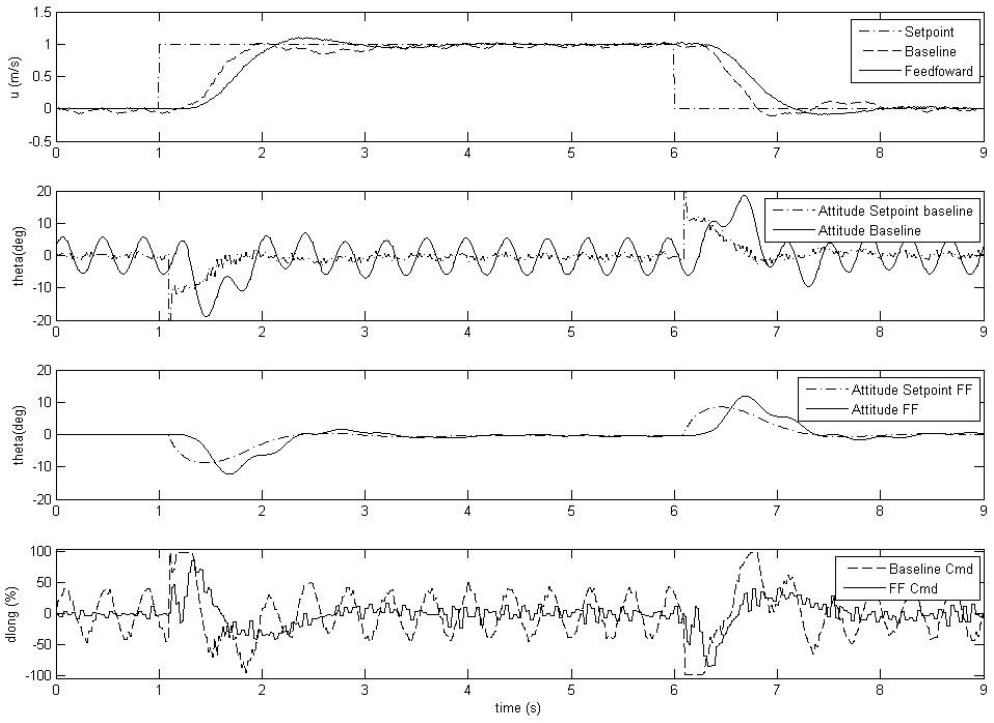

Fig. 11 HIL simulation; Longitudinal velocity 1 m/s step

Same considerations can be applied to the 5 m/s forward and lateral velocity steps (fig 12 and 14) and to 1 m/s lateral velocity step (fig 13). In the 5 m/s step velocities cases (fig 12 and fig.14), it has to be noticed that the feedforward controller achieves a reduced overshoot

amount even if the Baseline can count on the Derivative term of the PID. This can be explained considering that, during transients, the FF structure allows smaller errors in the inner attitude control loop.

Finally, in all performed tests, it has been observed a less oscillating behavior in the feedforward controller responses, justified by the greater stability margins that are, at least in this case, well better than the norm requirements [7].

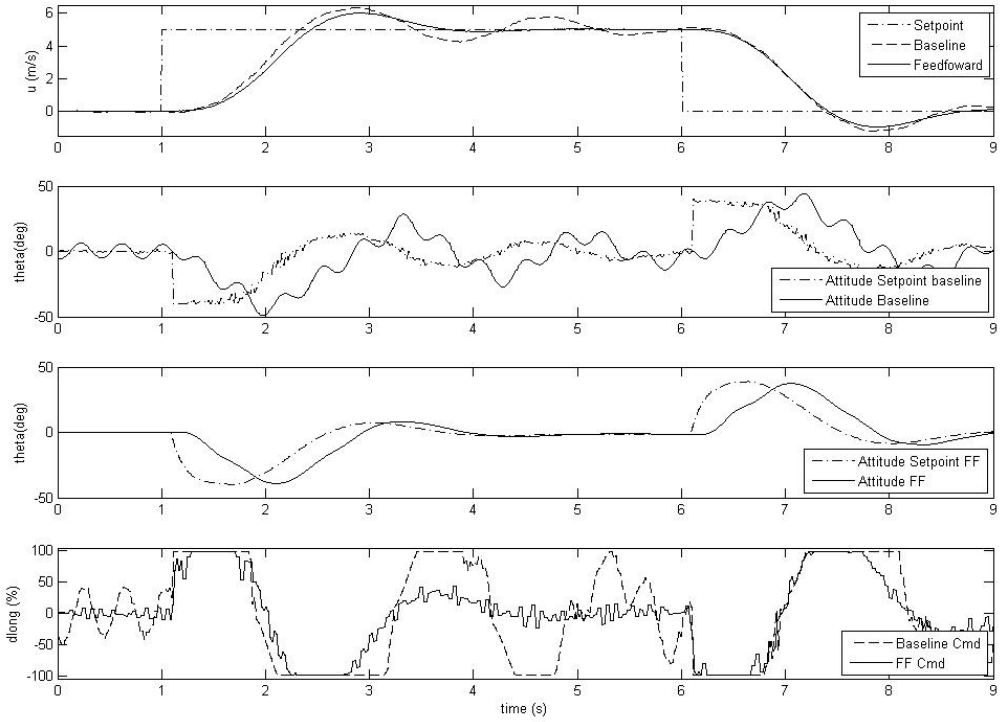

Fig. 12 HIL simulation; Longitudinal velocity 5 m/s step

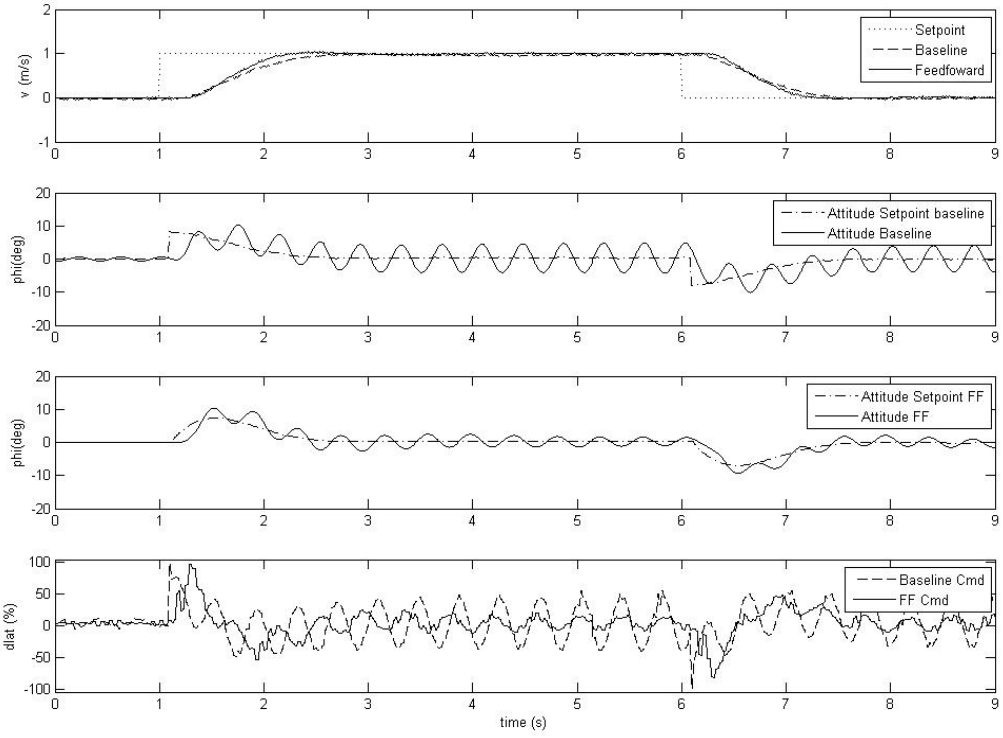

Fig. 13 HIL simulation; Lateral velocity 1 m/s step

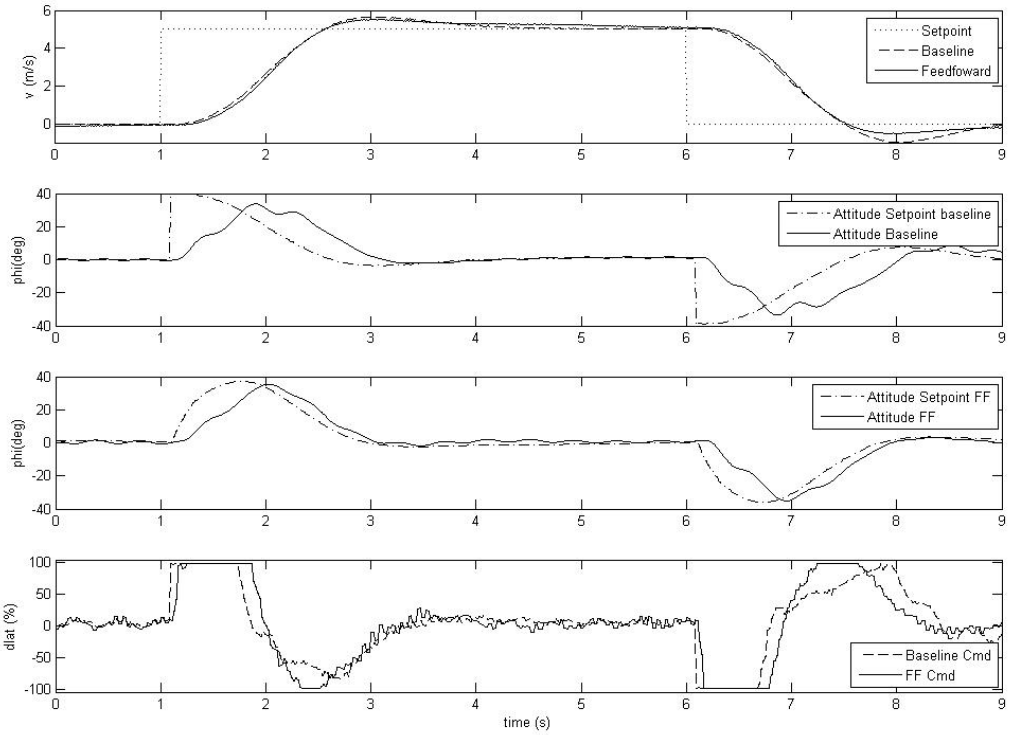

Fig. 14 HIL simulation; Lateral velocity 5 m/s step

H. Conclusion

In this paper results achieved using a model-based feed-forward controller designed for a small scale Helicopter in a Hardware In the Loop test bench simulations have been presented.

The FeedForward control architecture is based on nested proportional-integral control loops with a feedforward compensation in the inner loop and it has been described together with its smart discrete-time implementation. The feedforward term is obtained from the inversion of the command-attitude identified plant models.

Then, it has been demonstrated how this control combines benefits of feedforward and feedback controllers, and that it allows to reduce the number of parameters to be tuned from 12 to 10. Moreover it has been shown how feedforward action make the system work with smaller errors, with less saturation problems and allows an easier parameters tuning process. Comparisons upon performance and stability between the proposed FF controller and the Baseline one have been done using set of calibrations that have been automatically tuned in order to make an impartial analysis. Results have shown that, tuning the two systems for achieving the same performances, the feedforward controller works with higher stability margins and with less oscillating attitudes.

The presented analysis has been done by using a mathematical model of helicopter dynamics identified near low speed flight conditions. Anyway, since the dynamic model in forward flight conditions can be described by transfer functions of the same kind [4], this particular technique of control appears to be valid also in forward flight.

I. References

[1] B. Mettler, M.B. Tischler, and T. Kanade," Attitude Control Optimization for a Small-Scale Unmanned Helicopter ", AIAA Guidance, Navigation and Control Conference, 2000, pp. 40-59.

[2] R.Pretolani, G.M.Saggiani, V.Rossi, B.Teodorani "An "off the shelf" avionics system for Rotary Wing UAV rapid prototyping", Proceedings of the 32nd European Rotorcraft Forum, Sept. 2006, Maastrich, The Netherlands

[3] F.Zanetti , B. Teodorani , G.M.Saggiani, R.Pretolani, "Rotary Wing UAV System Identification for flight control design" European Rotorcraft Forum Conference 2007, 11-09-2007 Kazan, Russia

[4] B. Mettler, "Identification modeling and characteristics of miniature rotorcraft ", Kluwer Academic Publisher, Boston, M.A., USA, 2003

[5] Houpis-Lamont, "Digital control systems ", Mc Grow Hill Publisher, Boston, M.A., USA, 2003

[6] Ljung, L. System Identification: Theory for the User. Second edition. PTR Prentice Hall, Upper Saddle River, NJ,1999.

[7] Handling qualities requirements for military rotorcrafts .Techincal Report ADS-33D-PRF, United States Army, St-Louis Missouri, 1996